Multiomics profiling of buffy coat and plasma unveils etiology-specific signatures in hepatocellular carcinoma

Jiwon Hong[1,2,†], Jung Woo Eun[3,†], Geum Ok Baek[3], Jae Youn Cheong[3], Seryoung Park[1], Soon Sun Kim[3], Hyo Jung Cho[3,*], Su Bin Lim[1,2,*]

[1]Department of Biochemistry & Molecular Biology, Ajou University School of Medicine, Suwon 16499, Korea

[2]Department of Biomedical Sciences, Graduate School of Ajou University, Suwon 16499, Korea

[3]Department of Gastroenterology, Ajou University School of Medicine, Suwon 16499, South Korea

*** Corresponding authors**

Hyo Jung Cho, Department of Gastroenterology, Ajou University School of Medicine, Suwon 16499, South Korea.

Tel: +82-31-219-7824, Fax: +82-31-219-5999, E-mail: pilgrim8107@hanmail.net, ORCID: 0000-0003-4792-8335

Su Bin Lim, Department of Biochemistry & Molecular Biology, Ajou University School of Medicine, Suwon 16499, Korea.

Tel: +82-31-219-5056, Fax: +82-31-219-5059, E-mail: sblim@ajou.ac.kr, ORCID: 0000-0003-1752-7039

[†]These authors contributed equally to the manuscript as first authors.

Running title: Multiomics profiling of hepatocellular carcinoma

Abbreviations

AUC, area under the curve; CI, confidence interval; DE, differential expression; DEG, differentially expressed gene; DEP, differentially expressed protein; GO, Gene Ontology; HBV, hepatitis B virus; HBV-HCC, hepatitis B virus-associated hepatocellular carcinoma; HCC, hepatocellular carcinoma;

ILC, innate lymphoid cell; NV-HCC, non-viral-associated hepatocellular carcinoma; PBMC, peripheral blood mononuclear cell; RRHO, rank-rank hypergeometric overlap; VD, validation dataset; WTS, whole-transcriptome sequencing

ABSTRACT

Background/Aims

Hepatocellular carcinoma (HCC) is a leading cause of cancer mortality worldwide. Despite identification of several biomarkers for HCC diagnosis, challenges such as low sensitivity and intratumoral heterogeneity have impeded early detection, highlighting the need for etiology-specific blood biomarkers.

Methods

We generated whole-transcriptome sequencing (WTS) and targeted proteome data from buffy coat and plasma samples from HCC patients. By integrating etiological information on viral infection, we investigated the etiology-specific gene expression landscape at the blood level. Validation of differentially expressed genes (DEGs) was performed using publicly available RNA-seq datasets and qRT–PCR with AUC analyses.

Results

Differential expression analyses with multiomics data revealed distinct gene expression profiles between HBV-associated HCC and nonviral HCC, indicating the presence of etiology-specific blood biomarkers. The identified DEGs were validated across multiple independent datasets, underscoring their utility as biomarkers. Additionally, single-cell RNA-seq analysis of HCC confirmed differences in DEG expression across distinct immune cell types.

Conclusions

Our buffy coat WTS data and plasma proteome data may serve as reliable sources for identifying etiology-specific blood biomarkers of HCC and might contribute to discovery of therapeutic targets for HCC across different etiologies.

Keywords: hepatocellular carcinoma, buffy coat, plasma, transcriptomics, proteomics

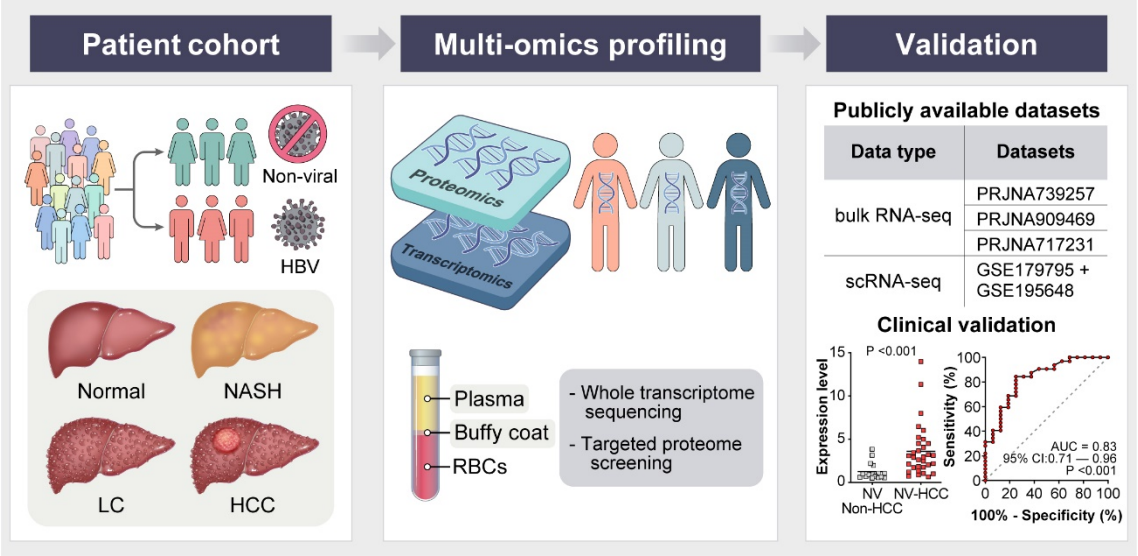

Highlights

- HBV-HCC and NV-HCC display distinct gene expression profiles compared to non-HCC at the buffy coat and plasma level.
- Validation by publicly available RNA-seq datasets and qRT–PCR confirms the reliability of the suggested etiology-specific HCC biomarkers.
- Single-cell RNA-seq analysis further confirms etiology-specific differences in DEG expression across distinct immune cell types found in blood.

INTRODUCTION

Hepatocellular carcinoma (HCC) is the fourth leading cause of cancer mortality worldwide [1]. HCC etiologies are classified into viral infection and nonviral causes [2]. Hepatitis B virus (HBV) is the main viral risk factor for HCC; nonviral causes include alcohol consumption and nonalcoholic fatty liver disease [2]. Most HCC patients are diagnosed at an advanced stage, for which curative treatments are limited [3]. Thus, proper HCC surveillance is important for early detection of HCC, which can lead to improved outcomes.

Diagnostic methods such as biopsy and imaging techniques combined with serum alpha-fetoprotein (AFP) level assessment have been frequently used in clinical practice but have several limitations, including low sensitivity and false positivity [4, 5]. Additionally, HCC is characterized by vast intertumoral heterogeneity induced by diverse etiologies and intratumoral heterogeneity owing to the tumor microenvironment [2, 6]. These limitations have emphasized the need for blood-based biomarkers to improve early detection of HCC, with a cell-free DNA signature and the combination of PIVKA-II and AFP as potential biomarkers [7, 8].

Gradient centrifugation separates blood into erythrocytes, the buffy coat, and plasma. The buffy coat is enriched in platelets and white blood cells, including peripheral blood mononuclear cells (PBMCs). PBMCs and plasma have been widely used for identification of blood-based biomarkers via transcriptomic and proteomic profiling [9, 10], including several blood-based HCC biomarkers [11, 12]. However, many limitations remain to be overcome, such as HCC heterogeneity caused by different etiologies [13]. Moreover, several studies have focused on transcriptome profiling using buffy coats to uncover altered gene signatures under disease conditions, including breast cancer and COVID-19 [14, 15]. Buffy coat analysis enables understanding whole-cell responses in peripheral blood against specific diseases, overcoming the limitation of exclusion of several cell types, such as granulocytes and circulating tumor cells, among PBMCs [16, 17]. However, buffy coat profiling of HCC blood-based biomarkers, particularly those related to HCC etiology, has not yet been conducted.

Hence, we aimed to identify etiology-specific blood biomarkers of HCC utilizing whole-transcriptome sequencing (WTS) and targeted proteome data from buffy coat and plasma samples obtained from HCC patients with diverse etiologies. We classified HCC patients into HBV-associated HCC (HBV-HCC) and nonviral-associated HCC (NV-HCC) groups according to etiology information. Compared to those of non-HCC samples, we investigated the etiology-specific gene expression landscape of HCC at the blood level via validation with publicly available RNA-seq datasets and qRT–PCR data from our buffy coat samples. We expect that our established multiomics dataset will serve as a reliable and reproducible source for identifying etiology-specific blood biomarkers of HCC and help in discovering potential therapeutic targets for HCC across different etiologies.

MATERIALS AND METHODS

Patient enrollment

Blood samples and data were obtained from the Biobank of Ajou University Hospital, Suwon, South Korea, between January 2017 and August 2023. All experiments in this study were conducted in accordance with the ethical guidelines of the 1975 Declaration of Helsinki. The study protocol was approved by the Institutional Review Board of Ajou University Hospital, Suwon, South Korea (AJOUIRB-EXP-2020-007). The requirement for informed consent was waived.

Blood sample preparation

Peripheral blood was collected from each individual directly into EDTA-containing tubes. The blood was centrifuged at 2000 × g for 5 min at 4°C, and the plasma or buffy coat was retained and aliquoted. Total RNA was isolated from buffy coats (300 μl) using TRIzol-LS (Invitrogen, Waltham, MA, USA) and purified using an RNeasy Mini kit (Qiagen, Hilden, Germany) according to the manufacturer's instructions. The RNA concentration and integrity were measured by an Agilent 2100 bioanalyzer (G2939A; Agilent Technologies, Santa Clara, CA, USA).

Whole transcriptome sequencing of buffy coat samples

The total RNA concentration was calculated by Quant-IT RiboGreen (Invitrogen, #R11490). The

integrity of the total RNA was assessed with a TapeStation RNA ScreenTape (Agilent, #5067-5576). Only high-quality RNA preparations with RIN greater than 7.0, were used for library construction. A library was independently prepared with an Illumina TruSeq Stranded Total RNA Library Prep Globin Kit (Illumina, San Diego, CA, USA, #20020613). Next, rRNA was removed using a Ribo-Zero rRNA Removal Kit (Human/Mouse/Rat Globin) (Illumina). The cleaved RNA fragments were converted to first-strand cDNA using SuperScript II reverse transcriptase (Invitrogen, #18064014) and random primers, followed by second-strand cDNA synthesis using DNA Polymerase I, RNase H and dUTP. The products were then purified and enriched via PCR to create the final cDNA library. The libraries were quantified using KAPA Library Quantification kits according to qPCR Quantification Protocol Guide (KAPA BIOSYSTEMS, #KK4854) and qualified using TapeStation D1000 ScreenTape (Agilent, #5067-5582). Indexed libraries were then subjected to an Illumina NovaSeq (Illumina) paired-end (2×100 bp) sequencing performed by Macrogen Incorporated.

Differential expression (DE) analyses of WTS data

The raw data (FASTQ) were imported into AltAnalyze software (v2.1.4), which uses the embedded software Kallisto and Ensemble72 annotations. Raw count values were obtained and used for DE analysis via R DESeq2 package (v1.34.0). Genes with a total read count less than 10 were excluded from further analysis. Differentially expressed genes (DEGs) were identified by pairwise comparison through DESeq2. Volcano plots were drawn using R EnhancedVolcano package (v1.12.0). Gene Ontology (GO) analysis was performed using R compareCluster function in clusterProfiler package (v4.2.2). The top 10 terms from either up-DEGs or down-DEGs are displayed in a dot plot.

DE analysis of validation datasets (VDs)

Bulk RNA-seq datasets of HCC PBMCs were downloaded from NCBI BioProject under accession codes PRJNA739257, PRJNA909469, and PRJNA717231. The raw data (FASTQ) were imported into AltAnalyze. Raw count values were obtained and used for DE analysis via R DESeq2 package. Genes with a total read count less than 1 were excluded from further analysis. The

significance of differences in expression of buffy coat DEGs was validated at p.adj<0.05. Count values were obtained by plotCounts function in DESeq2 and visualized as haploid plots by ggplot and geom_boxjitter functions in R ggplot2 (v3.4.2) and ggpol (v0.0.7) packages.

Rank-rank hypergeometric overlap (RRHO)

Log2-fold change values were obtained from DESeq2 results. All genes annotated in the buffy coat WTS and validation datasets were ranked by log fold change. These ranked lists were further processed to include only genes common to both the buffy coat and each VD. These input files were loaded into a simple web-based version of RRHO (https://systems.crump.ucla.edu/rankrank/rankranksimple.php). The step size was set to 100 to generate a Benjamini-Yekutieli-corrected hypergeometric matrix and RRHO heatmaps.

Targeted proteome screening of plasma samples

Plasma protein levels were measured using the proximity extension immunoassay technology (Olink Proteomics, Uppsala, Sweden) and an Olink® Target 96 Immuno-Oncology (v.3113) panel [18]. To conduct DE analysis, Normalized Protein eXpression files, log2 scale values, were imported into R OlinkAnalyze package (v3.4.1). Differentially expressed proteins (DEPs) were identified by pairwise comparison through olink_ttest function in OlinkAnalyze package. Volcano plots were drawn using R EnhancedVolcano package.

Single-cell RNA-seq analysis of the validation dataset

Targeted single-cell RNA-seq datasets of HCC from BD Rhapsody Immune Response Targeted Panel (human) were downloaded from NCBI Gene Expression Omnibus under accession codes GSE179795 and GSE195648. Gene expression matrices containing distribution-based error correction-adjusted molecule counts were imported into R Seurat package (v4.3.0.1). Single-cell QC was performed filtering for a total of 1,500 reads. Batch-balanced KNN correction was conducted using R bbknnR package (v1.0.2). Cells expressing CD19 or CD14 were excluded for elimination of contaminating B cells and monocytes. Clustering was repeated after filtering contaminating cells. Cell types were annotated using canonical markers reported in several recent

publications [19-23]. Violin plots were drawn using VlnPlot function in Seurat.

Quantitative reverse transcription PCR (qRT–PCR)

mRNA expression levels in buffy coat samples were measured using qRT–PCR. Buffy coat RNA was reverse transcribed to cDNA using SuperScript™ Ⅳ VILO™ Master Mix (Invitrogen). qRT–PCR was performed using amfiSure qGreen Q-PCR Master Mix (GenDEPOT, Barker, TX, USA) with individual primer sets (Supplementary Table S1) and monitored in real time using CFX Connect Real-Time PCR System (Bio-Rad Laboratories, Hercules, CA, USA). Relative gene expression levels were calculated using the $2^{-\Delta\Delta Ct}$ method, and GAPDH was used as the internal control. All measurements were performed in triplicate.

Area under the ROC curve (AUC) analysis

Receiver operating characteristic (ROC) analysis was performed using GraphPad Prism software (v10.0; GraphPad Software, San Diego, CA, USA), and the area under the ROC curve (AUC) was calculated, providing a quantitative measure of the overall diagnostic effectiveness. This analysis was complemented by 95% confidence intervals (CIs) for AUCs, offering a statistical range within which the true area under the curve is expected to lie and thereby indicating the precision of our assessment.

RESULTS

Study design

In our study, blood samples, along with etiology information, were obtained from healthy controls, nonalcoholic steatohepatitis patients, liver cirrhosis patients and HCC patients (Figure 1, Supplementary Table S2). After centrifugation, buffy coat and plasma samples were obtained for WTS and targeted proteome screening, respectively. In the transcriptome analysis, buffy coat samples were divided into HCC and non-HCC groups; in the proteome analysis, plasma samples were classified into HCC and healthy groups. For identification of etiology-specific biomarkers, the samples were subdivided into viral (HBV) or nonviral groups according to their HBV infection status. Using three comparison sets, DE analyses were performed to identify etiology-specific

DEGs and DEPs in HCC at the transcriptome and proteome levels. The identified DEGs were validated by analyzing publicly available bulk RNA-seq datasets of HCC PBMCs and performing qRT–PCR of buffy coat samples with AUC analysis. Further validation was conducted at the single-cell level using publicly available targeted scRNA-seq datasets.

DE analyses of buffy coat WTS data

To identify etiology-specific HCC biomarkers in the buffy coat transcriptome, we performed DE analyses comparing HCC and non-HCC samples from both HBV and nonviral groups. We further performed DE analysis between HBV-HCC and NV-HCC patients (Figure 2A). A total of 40 and 987 DEGs were identified in the HBV-HCC and NV-HCC samples, respectively, compared to the corresponding non-HCC samples ($p.adj<0.05$, $\log|FC|>0.5$). To investigate the etiology-derived functional distinctions of the identified DEGs, we performed GO analysis of the significant DEGs in each comparison ($p.adj<0.05$) (Figure 2B). In HBV-HCC, the significantly enriched GO terms are involved in immune responses, including regulation of the innate immune response and activation of immune cells. In contrast, the significantly enriched GO terms in NV-HCC are related to ATP metabolism and respiration. This tendency was corroborated by GO analysis between HBV-HCC and NV-HCC, with up-DEGs in HBV-HCC enriched in the immune response pathway and down-DEGs enriched in metabolism (Figure 2B). The significant DEGs ($p.adj<0.05$, $\log|FC|>0.5$) in the buffy coat transcriptome analysis are summarized in Figure 2C; these DEGs were either etiology specific or HCC specific, regardless of etiology, with overlapping expression patterns in the two comparisons.

Validation of buffy coat DEGs

To validate the reliability of our buffy coat transcriptome dataset, we utilized three publicly available RNA-seq datasets of HCC PBMCs. To our knowledge, buffy coat transcriptome data related to HCC have not yet been published. Hence, HCC PBMC datasets were used for validation of the DE results for buffy coats. This selection was motivated by the intrinsic proximity of PBMCs to the buffy coat, as PBMCs are conventionally derived from the buffy coat. In light of the limited number of publicly available HCC PBMC transcriptome datasets, with the majority

lacking comprehensive etiology information on HCC development, we identified three independent bulk RNA-seq datasets of HCC PBMCs. Notably, all datasets included samples from both HBV-associated HCC patients and healthy individuals (Supplementary Table S3). Through RRHO analysis [24], we assessed the overlap intensity between our buffy coat transcriptome dataset and each VD. For VD1 and VD2, a significant overlap was observed, whereas VD3 was shown to have a poor correlation with the buffy coat dataset (Figure 3A).

We analyzed the DEGs in each VD and compared each DE result with the buffy-coat DE result. Among the forty significant DEGs in the buffy coat transcriptome analysis of HBV-HCC patients compared to non-HCC patients, 27 genes were significantly differentially expressed in at least one VD (Figure 3B). In VD1-3, 20, 16, and 9 DEGs overlapped with buffy-coat DEGs (Figure 3B, Supplementary Figure S1). The overlapping DEGs in each dataset are summarized in Figure 3C with the total overlap frequency. Excluding HBA2, HBA1, and HBG2, which are considered to originate from erythrocyte contamination, a total of 24 genes overlapped with the buffy coat transcriptome, suggesting that our buffy coat dataset may be reliably used for HCC blood transcriptome analysis and that these genes have the potential to serve as blood biomarkers for HBV-HCC.

To investigate the diagnostic performance of the identified DEGs in discriminating HCC patients from non-HCC patients in clinical settings, we conducted qRT–PCR and AUC analysis of C1QA and SH3PXD2B, which were significant DEGs in the buffy coat WTS data and all VDs (Figure 3C-3E). No significant difference in qRT–PCR results for C1QA, which was upregulated in both HBV-HCC and NV-HCC in the buffy coat transcriptome, in HBV groups was detected, though it was significantly upregulated in NV-HCC, with an AUC of 0.68 (95% CI: 0.53-0.83, $P = 0.05$) (Figure 3D). SH3PXD2B, upregulated only in HBV-HCC in the buffy coat transcriptome, displayed significant upregulation in HBV-HCC based on qRT–PCR data, with an AUC of 0.73 (95% CI: 0.63-0.84, $P < 0.001$), representing its diagnostic potential as a blood biomarker for HBV-HCC (Figure 3E). Further examination using early-stage HCC samples compared to at-risk patients (NASH, LC) showed good diagnostic performance for detection of early-stage HBV-HCC using

SH3PXD2B, with an AUC of 0.74 (Supplementary Figure S2A, S2B).

DE analyses of targeted plasma proteome data

Next, plasma samples derived from HCC patients and healthy controls were subjected to targeted proteome screening for 92 immuno-oncology proteins to investigate etiology-specific HCC markers at the protein level. A total of 59 and 73 DEPs were identified in the HBV-HCC and NV-HCC patients, respectively, compared to the controls (Figure 4A, 4B). Compared with those in NV-HCC, a total of 6 proteins were significantly downregulated in HBV-HCC (Figure 4A). Most DEPs were upregulated in HCC samples compared to the control samples, regardless of HCC etiology, implying that immuno-oncology proteins are typically upregulated upon HCC development (Figure 4A). In contrast to the results of the transcriptome analysis, most of the DEPs overlapped between HBV-HCC and NV-HCC patients (Figure 4B). To examine the correlation between the transcriptome and proteome DE results, we confirmed the expression levels of significant DEPs at the transcriptome level using buffy-coat WTS data. Among the significant DEPs, six up-DEPs exhibited correlated expression patterns at the transcriptome and proteome levels (Figure 4C). Among the six DEPs, Gal-9 (LGALS9) and HO-1 (HMOX1) were HBV-HCC specific, while only CD70 was NV-HCC specific. Gal-1 (LGALS1) was not etiology specific but rather HCC specific for both HBV-HCC and NV-HCC patients.

These genes proven to be upregulated in HCC using multiomics data were examined by qRT–PCR and AUC analyses to further investigate their potential as biomarkers (Figure 4D-4F). Unexpectedly, HCC-specific Gal-1 was significantly downregulated in the HBV-HCC group, with an AUC of 0.68 (95% CI: 0.55-0.81, $P = 0.005$), but was significantly upregulated in the NV-HCC group, with an AUC of 0.73 (95% CI: 0.58-0.88, $P = 0.01$), implying that Gal-1 might serve as an NV-HCC-specific biomarker (Figure 4D). HBV-HCC-specific Gal-9 was significantly upregulated in patients with HBV-HCC, though it showed poor diagnostic value, with an AUC of 0.55 (95% CI: 0.44-0.67, $P = 0.4$) (Figure 4E). Notably, NV-HCC-specific CD70 was significantly upregulated in NV-HCC patients, with an AUC of 0.83 (95% CI: 0.71-0.96, $P < 0.001$), showing its superior potential as an NV-HCC-specific blood biomarker (Figure 4F). In addition, CD70 displayed great

diagnostic potential for detection of early-stage NV-HCC, with an AUC of 0.82 (Supplementary Figure S2C-S2E).

Single-cell analysis of the identified DEGs

To assess differences in DEG expression across distinct cell populations in blood, we processed and analyzed publicly available targeted single-cell RNA-seq datasets of innate lymphoid cells (ILCs) derived from patients with HBV-HCC and NV-HCC (see Methods). After batch-balanced KNN correction, seven clusters were identified, among which two were classified as T cells and four as ILCs (Figure 5A, 5B). The control and HBV-HCC patient cellular compositions exhibited considerable similarity, whereas NV-HCC patients displayed a distinct cellular profile characterized by an increased proportion of T cells and a reduced presence of ILC3 (Figure 5C).

We first examined expression levels of DEGs in the buffy coat transcriptome in each cell type and identified a total of 8 genes with expression patterns that correlated with those of the buffy coat transcriptome (Figure 5D, Supplementary Figure S3A). IFITM3, one of the up-DEGs in HBV-HCC, was significantly upregulated in CD8 T cells, NK cells, and ILCs compared to healthy controls. For NV-HCC, a total of 5 genes (ANXA5, CD63, ITGB2, JUN, and LGALS1) were significantly upregulated in different cell types but TCF7 was significantly downregulated in ILCs compared to control cells. Compared with that in NV-HCC, JUN was significantly downregulated in ILCs in HBV-HCC. Furthermore, we examined the cell type-specific expression levels of DEGs that exhibited correlating expression patterns at both the transcriptome and proteome levels (Figure 5E, Supplementary Figure S3B). HBV-HCC-specific Gal-9 was significantly upregulated in ILC1 of HBV-HCC. Additionally, HCC-specific Gal-1 was significantly upregulated in the ILCs of HBV-HCC patients (Figure 5E) and in the T cells and ILCs of NV-HCC patients (Figure 5D).

DISCUSSION

HCC accounts for more than 80% of primary liver cancers, and increasing evidence shows that chronic liver diseases such as nonalcoholic fatty liver disease and liver cirrhosis can contribute to HCC development [25, 26]. Since late detection of HCC is linked to limited therapeutic options [1],

differentiating between liver diseases by easy-to-use reliable biomarkers would greatly help to reduce HCC mortality [27]. Interestingly, recent studies have revealed distinct transcriptomic and immune profiles between viral HCC and nonviral HCC through RNA-seq analyses [28, 29], highlighting the importance of an etiology-specific understanding of HCC for effective diagnosis and treatment. Hence, we aimed to unveil etiology-specific blood signatures in HCC through multiomics profiling of buffy coats and plasma.

Our GO analysis revealed different profiles of significant DEGs according to HCC etiology. Given that NV-HCC is likely to develop from metabolic diseases because of excessive oxidative stress [30], it is reasonable that metabolic processes are enriched in NV-HCC. Indeed, oxidative phosphorylation has been defined as a major signal underlying HCC [31]. Additionally, energy metabolic processes such as ATP metabolism are altered in HCC [32] and might be exploited as therapeutic targets. However, most studies do not differentiate HCC by etiology. In our study, enriched metabolic processes were identified as characteristics of NV-HCC, whereas HBV-HCC was characterized by activated immune responses. It has been reported that the microenvironment of HBV-HCC is more immunosuppressive and exhausted than that of NV-HCC [29]. This might be linked to the different response rates to immune checkpoint inhibitors between HBV-HCC patients and NV-HCC patients. In general, patients with HBV-HCC have a better response rate [33]. These results suggest the need for differentiated strategies for HCC treatment and biomarker identification depending on etiology, particularly in cancer immunotherapy.

Among 24 DEGs in HBV-HCC identified through buffy coat WTS analyses combined with VDs, SH3PXD2B upregulation was repeatedly confirmed by all VDs and qRT–PCR with a high AUC, indicating its great potential as an effective blood biomarker for diagnosis of HBV-HCC. In addition, NV-HCC-specific CD70, as revealed by our multi-omics profiling, has not yet been studied regarding diagnostic values for HCC. CD70 upregulation in NV-HCC was confirmed by qRT–PCR, with a high AUC, suggesting that CD70 might serve as a novel NV-HCC-specific blood biomarker. Interestingly, CD70 has also been reported as an emerging target in cancer immunotherapy [34].

Notably, SH3PXD2B and CD70 displayed great diagnostic performance for detection of early-stage HCC compared to at-risk patients with NASH or cirrhosis, suggesting that profiling expression of these genes in the buffy coat can serve as an effective strategy for HCC surveillance. This approach may help to effectively distinguish HCC from chronic liver diseases that often share common signatures, such as cirrhosis, thereby enhancing early detection of HCC and consequently reducing HCC mortality [27]. Integrating these results, we suggest that SH3PXD2B and CD70 are potent blood-based biomarkers for HCC diagnosis and potential therapeutic targets across different etiologies.

Finally, we validated cell type-specific differences in DEG expression using publicly available targeted single-cell RNA-seq datasets. Although these datasets derived from ILCs isolated from the PBMCs of HCC patients, we identified a total of 7 cell clusters, including T cells, NK cells, and ILCs. The limited number of target genes and cell types included in the datasets precluded validation of SH3PXD2B and CD70, which are proposed as effective biomarkers with diagnostic potential. Unlike SH3PXD2B, CD70 was included in the targeted gene panel, but its expression in the identified cell types was not detected (Supplementary Figure S4A). Further investigation through the ABC portal [35] using healthy PBMCs suggested that CD70 was expressed in B cells and dendritic cells, though SH3PXD2B was not obviously detected (Supplementary Figure S4B). Despite these limitations, single-cell validation enabled us to investigate expression of multiple DEGs at the cell type level. Notably, IFITM3 was shown to be upregulated in all cell types except for CD4 T cells, emphasizing its reliability as a biomarker. Although the limited availability of single-cell RNA-seq datasets restricts validation of several genes at the single-cell level, their validation using bulk RNA-seq datasets and multiomics profiling emphasizes the effective utility of buffy coat mRNA signatures for HCC diagnosis.

Overall, we discerned etiology-specific blood biomarkers for HCC by employing multiomics profiling, incorporating buffy coat WTS and targeted plasma proteome data. This identification was corroborated through validation using publicly available bulk RNA-seq and single-cell RNA-seq datasets and conducting qRT–PCR with AUC analysis. Our investigation confirmed distinctive

gene expression landscapes for HCC across different etiologies at the blood level, suggesting that several genes, particularly SH3PXD2B and CD70, are novel etiology-specific blood biomarkers. Our comprehensive multiomics profiling and validation across diverse datasets may serve as a resource for identifying etiology-specific blood biomarkers for HCC, with the potential to be effectively applied in clinical settings, and for facilitating exploration of etiology-specific therapeutic targets.

Acknowledgments

The biospecimens and corresponding clinical information were provided by the Biobank of Ajou University Hospital, a member of the Korea Biobank Network. S.B.L. is supported by the National Research Foundation (NRF) of Korea (2020M3A9D8037604, 2020R1A6A1A03043539, 2022R1A2C1008793, and 2022R1C1C1004756) and the Korea Health Technology R&D Project of the Korea Health Industry Development Institute (KHIDI), funded by the Ministry of Health & Welfare, Republic of Korea (HR22C1734). H.C.J is supported by the National Research Foundation (NRF) of Korea (NRF-2021R1C1C1009619) and the Korea Health Technology R&D Project of the Korea Health Industry Development Institute (KHIDI), funded by the Ministry of Health & Welfare, Republic of Korea (HR22C1734). J.W.E. is supported by the National Research Foundation (NRF) of Korea (2022R1A2C2092422) and the 2023 Regional Industry-linked University Open-Lab Development Support Program through the Commercializations Promotion Agency for R&D Outcomes (COMPA) funded by the Ministry of Science and ICT. and the Korea Health Technology R&D Project of the Korea Health Industry Development Institute (KHIDI), funded by the Ministry of Health & Welfare, Republic of Korea (HR21C1003).

Authors contributions

Conceptualization: JH, JWE, HJC, SBL. Data Curation: JH. Formal Analysis: JH, JWE. Funding Acquisition: HJC, SBL. Investigation: JH, JWE, SP, HJC, SBL. Project Administration: HJC, SBL. Resources: JWE, GOB, JYC, SSK, HJC, SBL. Supervision: HJC, SBL. Validation: JWE, GOB. Visualization: JH. Writing – original draft: JH, JWE, GOB, SP, HJC, SBL. Writing – review & editing: JH, JWE, GOB, SP, HJC, SBL. All authors have read and approved the final manuscript.

Conflicts of interest

The authors have no conflicts to disclose.

REFERENCES

1. Sankar K, Gong J, Osipov A, Miles SA, Kosari K, Nissen NN, et al. Recent advances in the management of hepatocellular carcinoma. Clin Mol Hepatol. 2024;30(1):1-15.

2. Chidambaranathan-Reghupaty S, Fisher PB, Sarkar D. Hepatocellular carcinoma (HCC): Epidemiology, etiology and molecular classification. Adv Cancer Res. 2021;149:1-61.

3. Kulik L, El-Serag HB. Epidemiology and Management of Hepatocellular Carcinoma. Gastroenterology. 2019;156(2):477-91.e1.

4. Elderkin J, Al Hallak N, Azmi AS, Aoun H, Critchfield J, Tobon M, et al. Hepatocellular Carcinoma: Surveillance, Diagnosis, Evaluation and Management. Cancers (Basel). 2023;15(21).

5. Parikh ND, Tayob N, Singal AG. Blood-based biomarkers for hepatocellular carcinoma screening: Approaching the end of the ultrasound era? J Hepatol. 2023;78(1):207-16.

6. Liu J, Dang H, Wang XW. The significance of intertumor and intratumor heterogeneity in liver cancer. Exp Mol Med. 2018;50(1):e416.

7. Kim SC, Kim DW, Cho EJ, Lee JY, Kim J, Kwon C, et al. A circulating cell-free DNA methylation signature for the detection of hepatocellular carcinoma. Mol Cancer. 2023;22(1):164.

8. Kim DY, Toan BN, Tan CK, Hasan I, Setiawan L, Yu ML, et al. Utility of combining PIVKA-II and AFP in the surveillance and monitoring of hepatocellular carcinoma in the Asia-Pacific region. Clin Mol Hepatol. 2023;29(2):277-92.

9. Han Z, Feng W, Hu R, Ge Q, Ma W, Zhang W, et al. RNA-seq profiling reveals PBMC RNA as a potential biomarker for hepatocellular carcinoma. Sci Rep. 2021;11(1):17797.

10. Ding Z, Wang N, Ji N, Chen ZS. Proteomics technologies for cancer liquid biopsies. Mol Cancer. 2022;21(1):53.

11. Kunadirek P, Pinjaroen N, Nookaew I, Tangkijvanich P, Chuaypen N. Transcriptomic Analyses Reveal Long Non-Coding RNA in Peripheral Blood Mononuclear Cells as a Novel Biomarker for Diagnosis and Prognosis of Hepatocellular Carcinoma. Int J Mol Sci. 2022;23(14).

12. Li J, Lv M, Huang Q, Hu R, Zhong X, Sun X, et al. FAT4 expression in peripheral blood mononuclear cells is associated with prognosis and immune cell infiltration in hepatocellular carcinoma. Sci Rep. 2023;13(1):15735.

13. Song T, Li L, Wu S, Liu Y, Guo C, Wang W, et al. Peripheral Blood Genetic Biomarkers

for the Early Diagnosis of Hepatocellular Carcinoma. Front Oncol. 2021;11:583714.

14. Donzelli S, Blandino G, Muti P. Use of Buffy Coat miRNA Profiling for Breast Cancer Prediction in Healthy Women. Methods Mol Biol. 2016;1379:13-9.

15. Cavalcante LTF, da Fonseca GC, Amado Leon LA, Salvio AL, Brustolini OJ, Gerber AL, et al. Buffy Coat Transcriptomic Analysis Reveals Alterations in Host Cell Protein Synthesis and Cell Cycle in Severe COVID-19 Patients. Int J Mol Sci. 2022;23(21).

16. He D, Yang CX, Sahin B, Singh A, Shannon CP, Oliveria JP, et al. Whole blood vs PBMC: compartmental differences in gene expression profiling exemplified in asthma. Allergy Asthma Clin Immunol. 2019;15:67.

17. Das DK, Naidoo MK, Ilboudo A, DuBois P, Durojaiye V, Liu C, et al. Isolation and Propagation of Circulating Tumor Cells from a Mouse Cancer Model. J Vis Exp. 2015(104).

18. Wik L, Nordberg N, Broberg J, Björkesten J, Assarsson E, Henriksson S, et al. Proximity Extension Assay in Combination with Next-Generation Sequencing for High-throughput Proteome-wide Analysis. Mol Cell Proteomics. 2021;20:100168.

19. Roma S, Carpen L, Raveane A, Bertolini F. The Dual Role of Innate Lymphoid and Natural Killer Cells in Cancer. from Phenotype to Single-Cell Transcriptomics, Functions and Clinical Uses. Cancers (Basel). 2021;13(20).

20. Spits H, Bernink JH, Lanier L. NK cells and type 1 innate lymphoid cells: partners in host defense. Nat Immunol. 2016;17(7):758-64.

21. Vivier E, Artis D, Colonna M, Diefenbach A, Di Santo JP, Eberl G, et al. Innate Lymphoid Cells: 10 Years On. Cell. 2018;174(5):1054-66.

22. Björklund Å K, Forkel M, Picelli S, Konya V, Theorell J, Friberg D, et al. The heterogeneity of human CD127(+) innate lymphoid cells revealed by single-cell RNA sequencing. Nat Immunol. 2016;17(4):451-60.

23. Sun Z, Li Y, Zhang Z, Fu Y, Han X, Hu Q, et al. CD160 Promotes NK Cell Functions by Upregulating Glucose Metabolism and Negatively Correlates With HIV Disease Progression. Front Immunol. 2022;13:854432.

24. Plaisier SB, Taschereau R, Wong JA, Graeber TG. Rank-rank hypergeometric overlap: identification of statistically significant overlap between gene-expression signatures. Nucleic

Acids Res. 2010;38(17):e169.

25. 2022 KLCA-NCC Korea practice guidelines for the management of hepatocellular carcinoma. Clin Mol Hepatol. 2022;28(4):583-705.

26. Seif El Dahan K, Daher D, Singal AG. Hepatocellular carcinoma surveillance in patients with non-alcoholic fatty liver disease. Clin Mol Hepatol. 2023;29(Suppl):S207-s19.

27. Sohn W, Kang D, Kang M, Guallar E, Cho J, Paik YH. Impact of nationwide hepatocellular carcinoma surveillance on the prognosis in patients with chronic liver disease. Clin Mol Hepatol. 2022;28(4):851-63.

28. Paslaru L, Bindea G, Nastase A, Sorop A, Zimbru C, Herlea V, et al. Comparative RNA-Sequencing Analysis Reveals High Complexity and Heterogeneity of Transcriptomic and Immune Profiles in Hepatocellular Carcinoma Tumors of Viral (HBV, HCV) and Non-Viral Etiology. Medicina (Kaunas). 2022;58(12).

29. Lim CJ, Lee YH, Pan L, Lai L, Chua C, Wasser M, et al. Multidimensional analyses reveal distinct immune microenvironment in hepatitis B virus-related hepatocellular carcinoma. Gut. 2019;68(5):916-27.

30. Van Thiel DH, Ramadori G. Non-viral causes of hepatocellular carcinoma. J Gastrointest Cancer. 2011;42(4):191-4.

31. Kudo Y, Sugimoto M, Arias E, Kasashima H, Cordes T, Linares JF, et al. PKCλ/ι Loss Induces Autophagy, Oxidative Phosphorylation, and NRF2 to Promote Liver Cancer Progression. Cancer Cell. 2020;38(2):247-62.e11.

32. Tenen DG, Chai L, Tan JL. Metabolic alterations and vulnerabilities in hepatocellular carcinoma. Gastroenterol Rep (Oxf). 2021;9(1):1-13.

33. Meyer T, Galani S, Lopes A, Vogel A. Aetiology of liver disease and response to immune checkpoint inhibitors: An updated meta-analysis confirms benefit in those with non-viral liver disease. J Hepatol. 2023;79(2):e73-e6.

34. Jacobs J, Deschoolmeester V, Zwaenepoel K, Rolfo C, Silence K, Rottey S, et al. CD70: An emerging target in cancer immunotherapy. Pharmacol Ther. 2015;155:1-10.

35. Gao X, Hong F, Hu Z, Zhang Z, Lei Y, Li X, et al. ABC portal: a single-cell database and web server for blood cells. Nucleic Acids Res. 2023;51(D1):D792-d804.

Figure legends

Figure 1. Schematics of the study design. Buffy coat and plasma samples extracted from healthy controls, nonalcoholic steatohepatitis (NASH) patients, liver cirrhosis (LC) patients and HCC patients were used for differential expression analyses. Buffy coats were used for whole-transcriptome sequencing (WTS); plasma was used for targeted proteome screening. All samples were assigned to HBV or nonviral groups according to etiology. Validation of DEGs was performed through publicly available bulk RNA-seq and scRNA-seq datasets and qRT–PCR with AUC analysis.

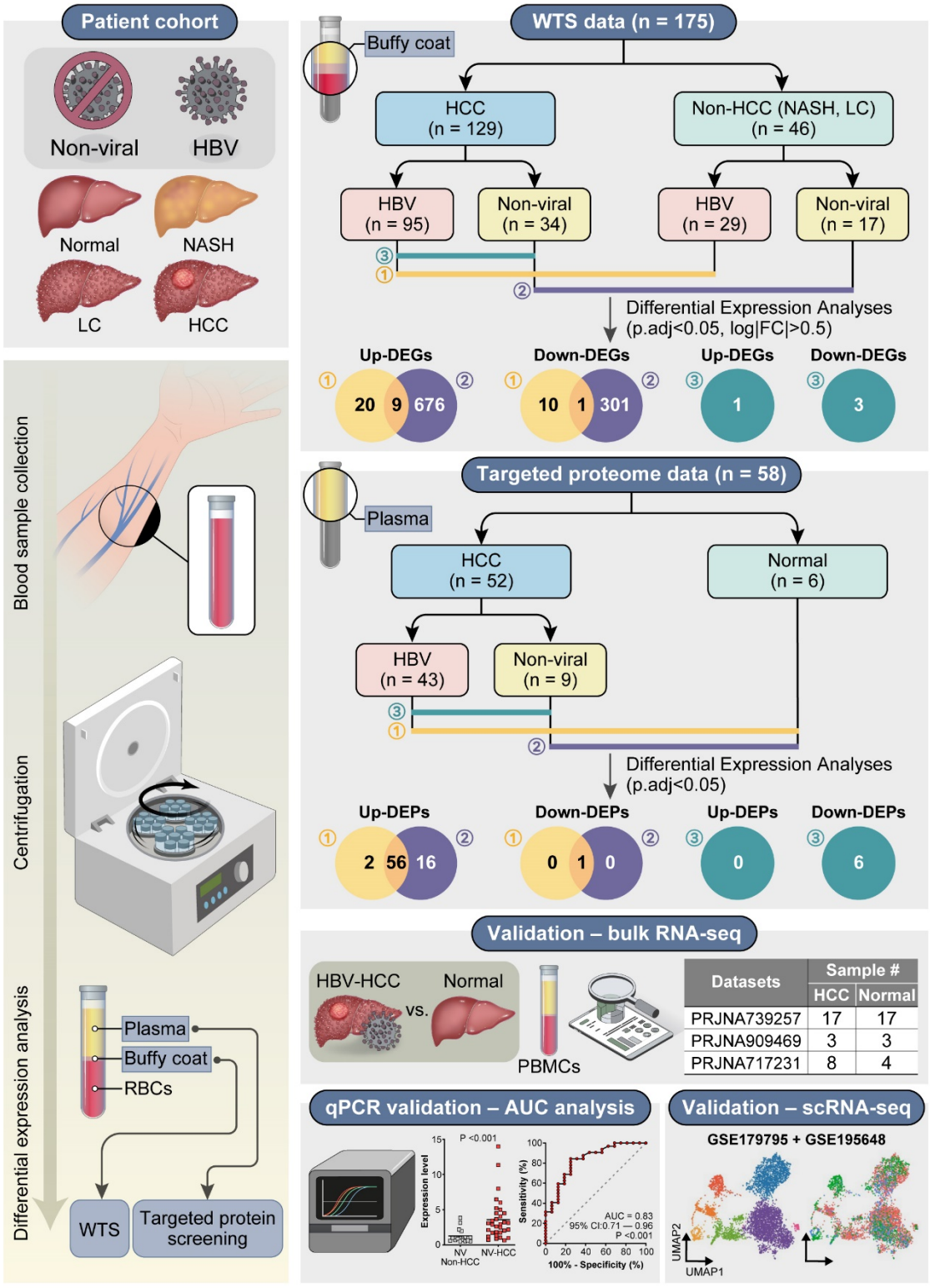
Patient cohort
Non-viral
HBV
Normal
NASH
LC
HCC
Blood sample collection
Centrifugation
Differential expression analysis
Plasma
Buffy coat
RBCs
WTS
Targeted protein screening
WTS data (n = 175)
Buffy coat
HCC (n = 129)
Non-HCC (NASH, LC) (n = 46)
HBV (n = 95)
Non-viral (n = 34)
HBV (n = 29)
Non-viral (n = 17)
Differential Expression Analyses (p.adj<0.05, log|FC|>0.5)
Up-DEGs
Down-DEGs
Up-DEGs
Down-DEGs
20 9 676
10 1 301
1
3
Targeted proteome data (n = 58)
Plasma
HCC (n = 52)
Normal (n = 6)
HBV (n = 43)
Non-viral (n = 9)
Differential Expression Analyses (p.adj<0.05)
Up-DEPs
Down-DEPs
Up-DEPs
Down-DEPs
2 56 16
0 1 0
0
6
Validation – bulk RNA-seq
HBV-HCC
vs.
Normal
PBMCs
Datasets
Sample #
HCC
Normal
PRJNA739257 17 17
PRJNA909469 3 3
PRJNA717231 8 4
qPCR validation – AUC analysis
P <0.001
Expression level
NV
NV-HCC
Non-HCC
Sensitivity (%)
AUC = 0.83
95% CI:0.71 — 0.96
P <0.001
100% - Specificity (%)
Validation – scRNA-seq
GSE179795 + GSE195648
UMAP2
UMAP1

Figure 2. DE analysis between HCC and non-HCC samples of HBV-HCC and NV-HCC using WTS data derived from buffy coats. (A) Volcano plots visualizing significant DEGs. (B) GO results showing enriched biological processes of significant up-DEGs and down-DEGs. (C) Venn diagrams summarizing significant up-DEGs and down-DEGs.

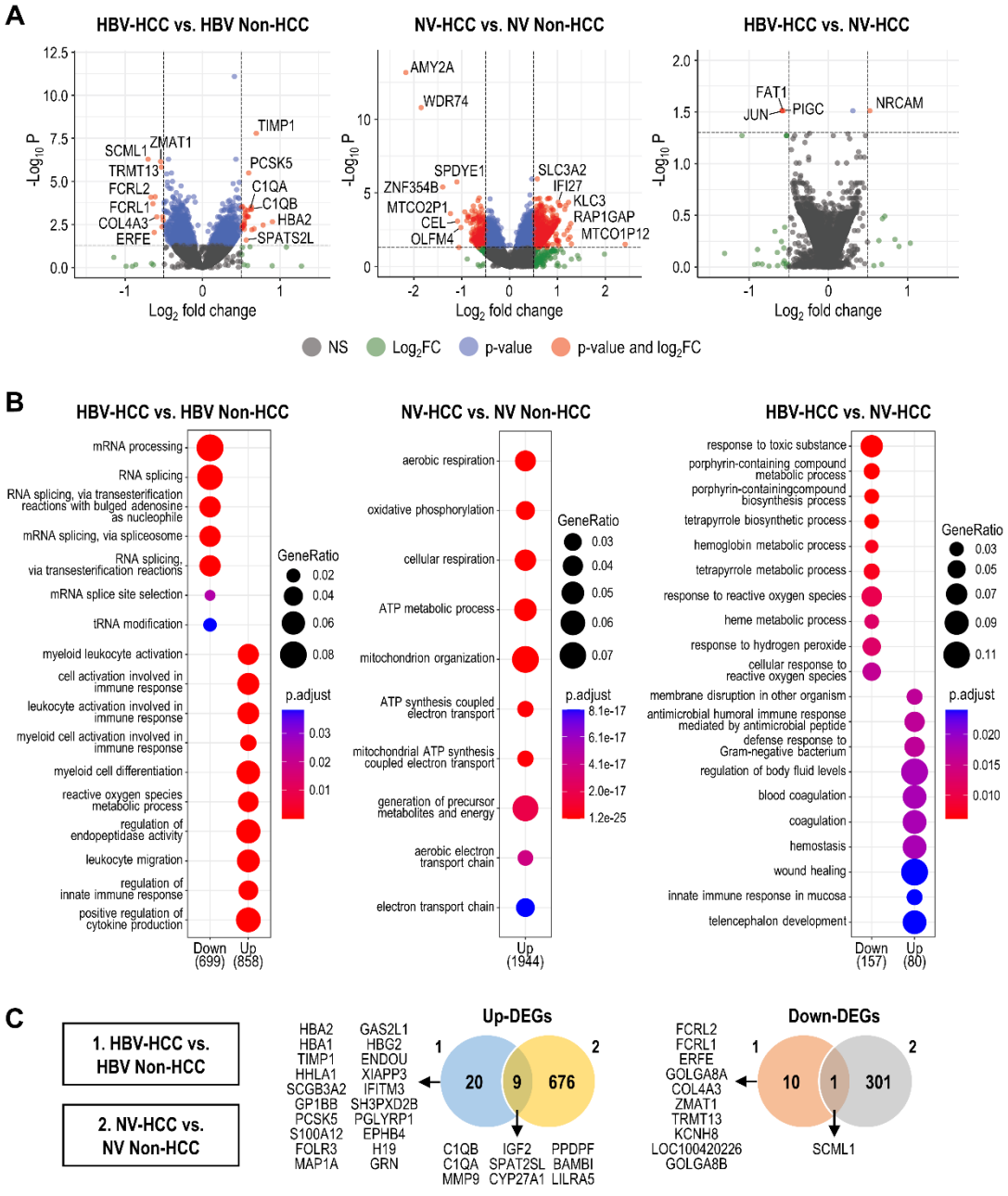
A
HBV-HCC vs. HBV Non-HCC
NV-HCC vs. NV Non-HCC
HBV-HCC vs. NV-HCC
-Log10 P
Log2 fold change
SCML1
ZMAT1
TRMT13
FCRL2
FCRL1
COL4A3
ERFE
TIMP1
PCSK5
C1QA
C1QB
HBA2
SPATS2L
AMY2A
WDR74
SPDYE1
ZNF354B
MTCO2P1
CEL
OLFM4
SLC3A2
IFI27
KLC3
RAP1GAP
MTCO1P12
FAT1
JUN
PIGC
NRCAM
NS
Log2FC
p-value
p-value and log2FC
B
HBV-HCC vs. HBV Non-HCC
NV-HCC vs. NV Non-HCC
HBV-HCC vs. NV-HCC
mRNA processing
RNA splicing
RNA splicing, via transesterification reactions with bulged adenosine as nucleophile
mRNA splicing, via spliceosome
RNA splicing, via transesterification reactions
mRNA splice site selection
tRNA modification
myeloid leukocyte activation
cell activation involved in immune response
leukocyte activation involved in immune response
myeloid cell activation involved in immune response
myeloid cell differentiation
reactive oxygen species metabolic process
regulation of endopeptidase activity
leukocyte migration
regulation of innate immune response
positive regulation of cytokine production
Down (699)
Up (858)
GeneRatio
p.adjust
aerobic respiration
oxidative phosphorylation
cellular respiration
ATP metabolic process
mitochondrion organization
ATP synthesis coupled electron transport
mitochondrial ATP synthesis coupled electron transport
generation of precursor metabolites and energy
aerobic electron transport chain
electron transport chain
Up (1944)
response to toxic substance
porphyrin-containing compound metabolic process
porphyrin-containingcompound biosynthesis process
tetrapyrrole biosynthetic process
hemoglobin metabolic process
tetrapyrrole metabolic process
response to reactive oxygen species
heme metabolic process
response to hydrogen peroxide
cellular response to reactive oxygen species
membrane disruption in other organism
antimicrobial humoral immune response mediated by antimicrobial peptide
defense response to Gram-negative bacterium
regulation of body fluid levels
blood coagulation
coagulation
hemostasis
wound healing
innate immune response in mucosa
telencephalon development
Down (157)
Up (80)
C
1. HBV-HCC vs. HBV Non-HCC
2. NV-HCC vs. NV Non-HCC
Up-DEGs
HBA2 HBA1 TIMP1 HHLA1 SCGB3A2 GP1BB PCSK5 S100A12 FOLR3 MAP1A
GAS2L1 HBG2 ENDOU XIAPP3 IFITM3 SH3PXD2B PGLYRP1 EPHB4 H19 GRN
20
9
676
C1QB C1QA MMP9
IGF2 SPAT2SL CYP27A1
PPDPF BAMBI LILRA5
Down-DEGs
FCRL2 FCRL1 ERFE GOLGA8A COL4A3 ZMAT1 TRMT13 KCNH8 LOC100420226 GOLGA8B
10
1
301
SCML1

Figure 3. Validation through RRHO and qPCR–AUC analyses. (A) RRHO heatmaps visualizing the overlap intensity between buffy coat WTS- and each VD-derived list of genes ranked by DE. The log fold changes are plotted in a bar graph along the x- and y-axes. (B) A table displaying significant DEGs in HBV-HCC vs. HBV-non-HCC patients validated by each VD. (C) Dot plot visualizing the overlapping number of significant DEGs in the HBV-HCC group vs. the HBV-non-HCC group compared with the VD group. (D-E) qRT–PCR and AUC results displaying the diagnostic performance of the identified DEGs. (D) C1QA results in HBV-HCC and NV-HCC. (E) SH3PXD2B results in HBV-HCC.

A

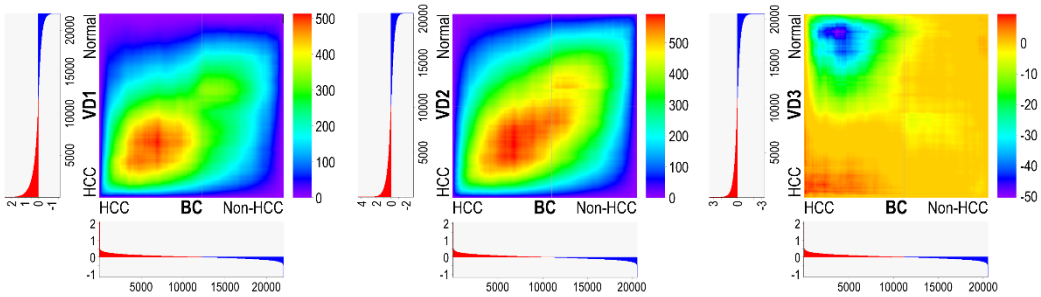

B

Comparison (transcriptome)		VD1	VD2	VD3
HBV-HCC vs. HBV Non-HCC (Up-DEGs)	HBV	HBA2, HBA1, TIMP1, GP1BB, PCSK5, S100A12, FOLR3, MAP1A, GAS2L1, HBG2, IFITM3, SH3PXD2B, PGLYRP1, GRN	TIMP1, GP1BB, S100A12, SH3PXD2B, PGLYRP1, GRN	HBA2, HBA1, GP1BB, SH3PXD2B, H19
	Both	C1QB, C1QA, MMP9, CYP27A1, BAMBI, LILRA5	C1QB, C1QA, CYP27A1, BAMBI, LILRA5	C1QB, C1QA, MMP9, PPDPF
HBV-HCC vs. HBV Non-HCC (Down-DEGs)	HBV	<NA>	FCRL1, COL4A3, TRMT13, KCNH8	<NA>
	Both	<NA>	SCML1	<NA>

C

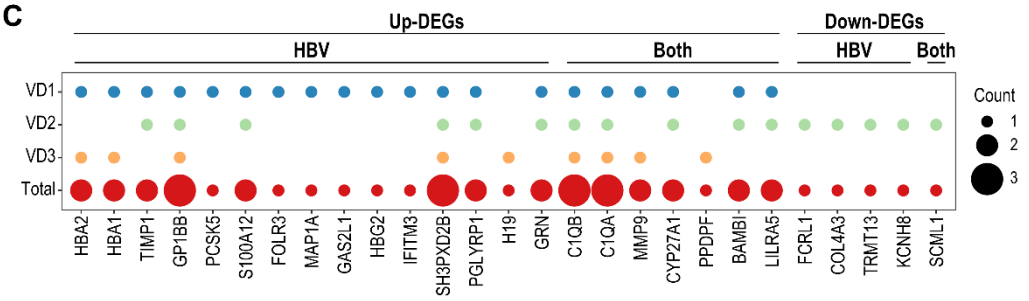

D

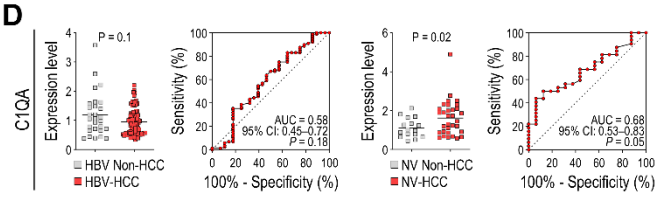

E

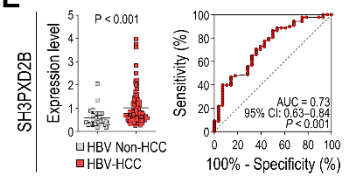

Figure 4. Proteome screening for targeted immuno-oncology genes using plasma samples. (A) Volcano plots visualizing significant DEPs. (B) Venn diagrams summarizing significant up-DEPs and down-DEPs. The list of significant DEPs is provided. (C) A table summarizing significant DEPs with correlating significant DE patterns in buffy-coat WTS data. Haploid plots of the transcriptome expression levels of each DEP are displayed together. (D-F) qRT–PCR and AUC results displaying the diagnostic performance of the identified DEPs at the mRNA level. (D) LGALS1 results in HBV-HCC and NV-HCC. (E) LGALS9 results in HBV-HCC. (F) CD70 results in NV-HCC.

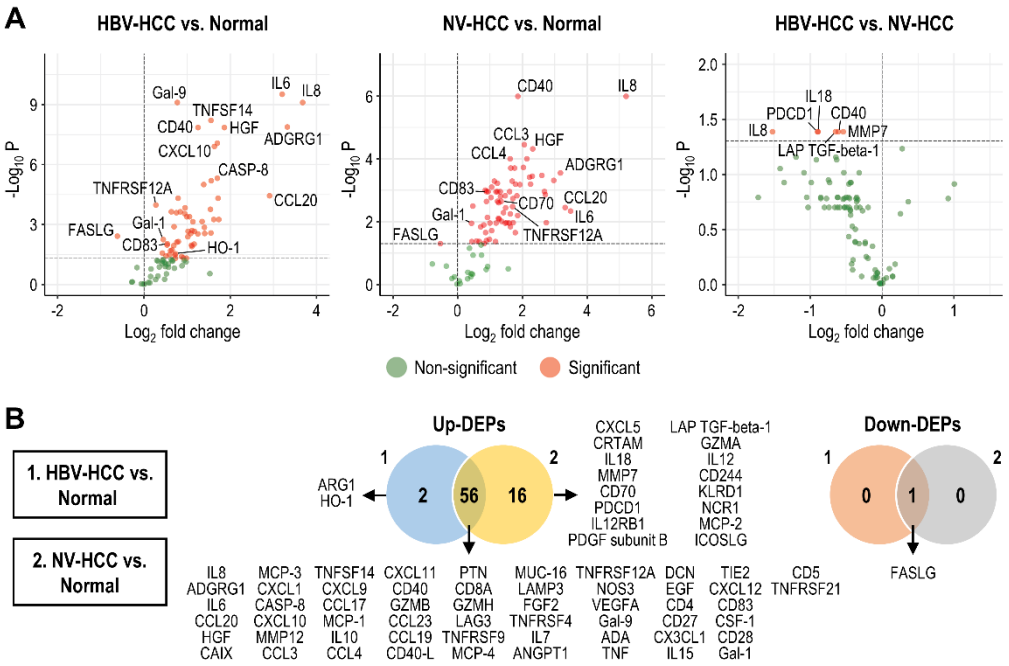

C

Comparison (proteome)		Buffycoat
HBV-HCC vs. Normal (Up-DEPs)	HBV	Gal-9, HO-1
	Both	Gal-1
NV-HCC vs. Normal (Up-DEPs)	NV	CD70
	Both	TNFRSF12A, CD83, Gal-1

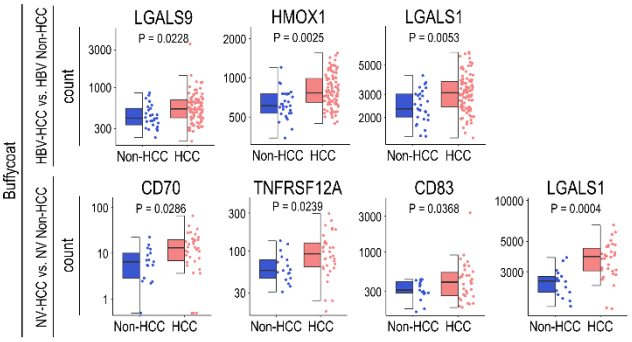

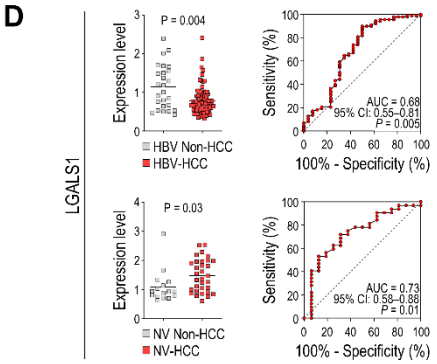

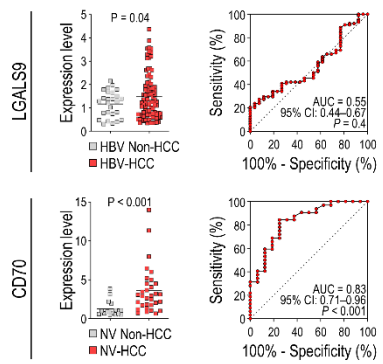

Figure 5. Single-cell analysis of the identified DEGs from multiomics profiling data. (A) UMAP visualizing cell clusters after correction. (B) Violin plots showing relative expression of cell type markers. (C) Stacked bar plot visualizing the composition of cell type proportions. (D) A table summarizing significant DEGs from the buffy coat analysis that had significant DE patterns across individual cell types, as displayed with violin plots showing the relative expression level of each gene in the specified cell types. (E) A table summarizing significant DEGs identified from the buffy coat and plasma multiomics analyses that exhibited significant DE patterns across individual cell types, as displayed with violin plots showing the relative expression level of each gene in the specified cell types.

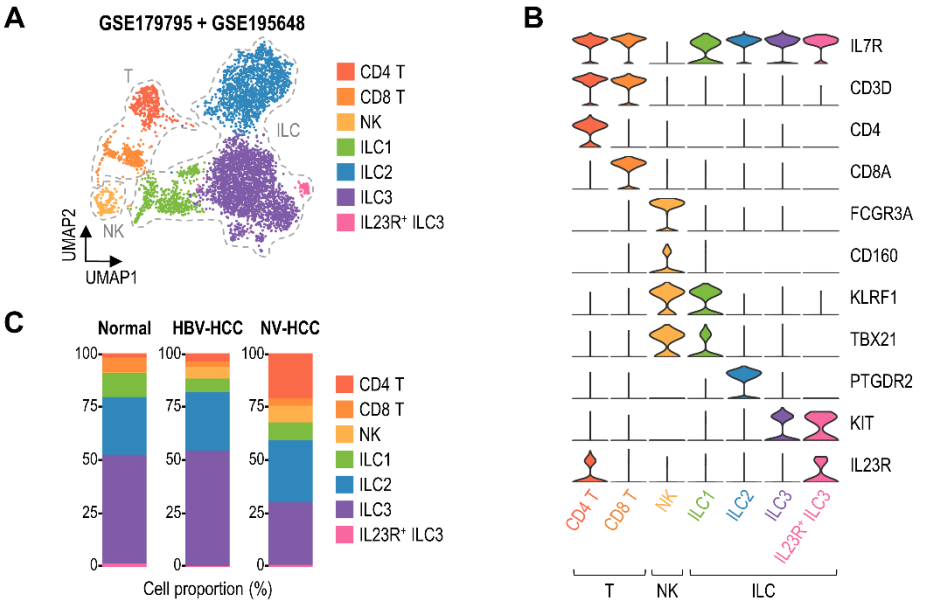

D

Comparison (transcriptome)	scRNA-seq
HBV-HCC vs. Non-HCC (Up-DEGs)	IFITM3
NV-HCC vs. Non-HCC (Up-DEGs)	ANXA5, CD63, ITGB2, JUN, LGALS1
NV-HCC vs. Non-HCC (Down-DEGs)	TCF7
HBV-HCC vs. NV-HCC (Down-DEGs)	JUN

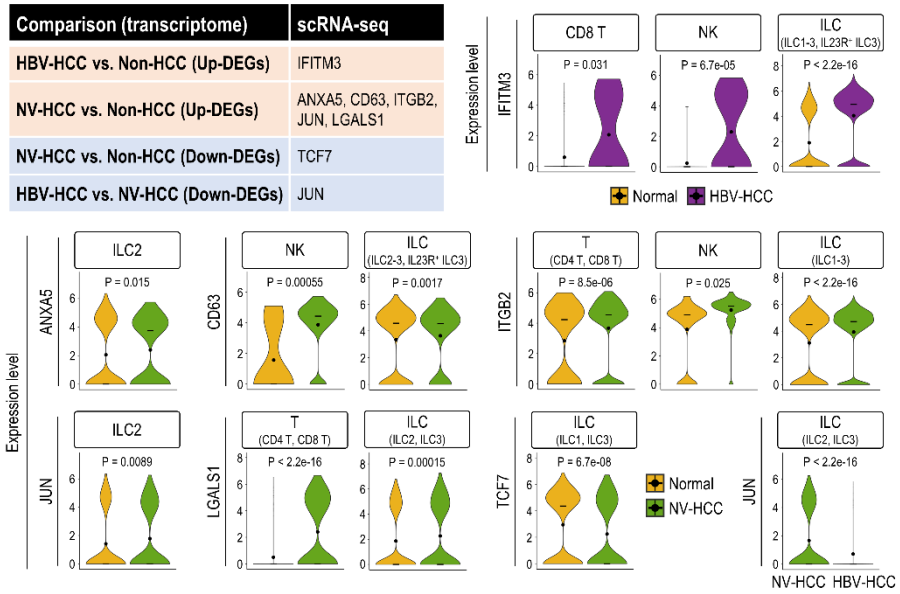

E

Comparison (proteome)	Buffycoat	scRNA-seq
HBV-HCC vs. Normal (Up-DEPs)	HBV	Gal-9, HO-1	Gal-9
	Both	Gal-1	Gal-1
NV-HCC vs. Normal (Up-DEPs)	NV	CD70	
	Both	TNFRSF12A, CD83, Gal-1	Gal-1

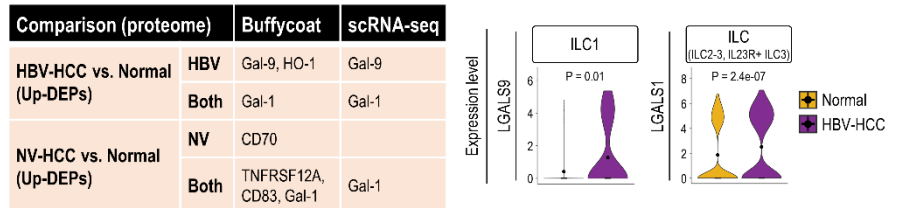

Supplementary materials

Supplementary Figure S1. Haploid plots for DEG expression from each validation dataset. (A-C) Haploid plots displaying the gene expression level of each significant DEG. (A) DEGs from VD1. (B) DEGs from VD2. (C) DEGs from VD3.

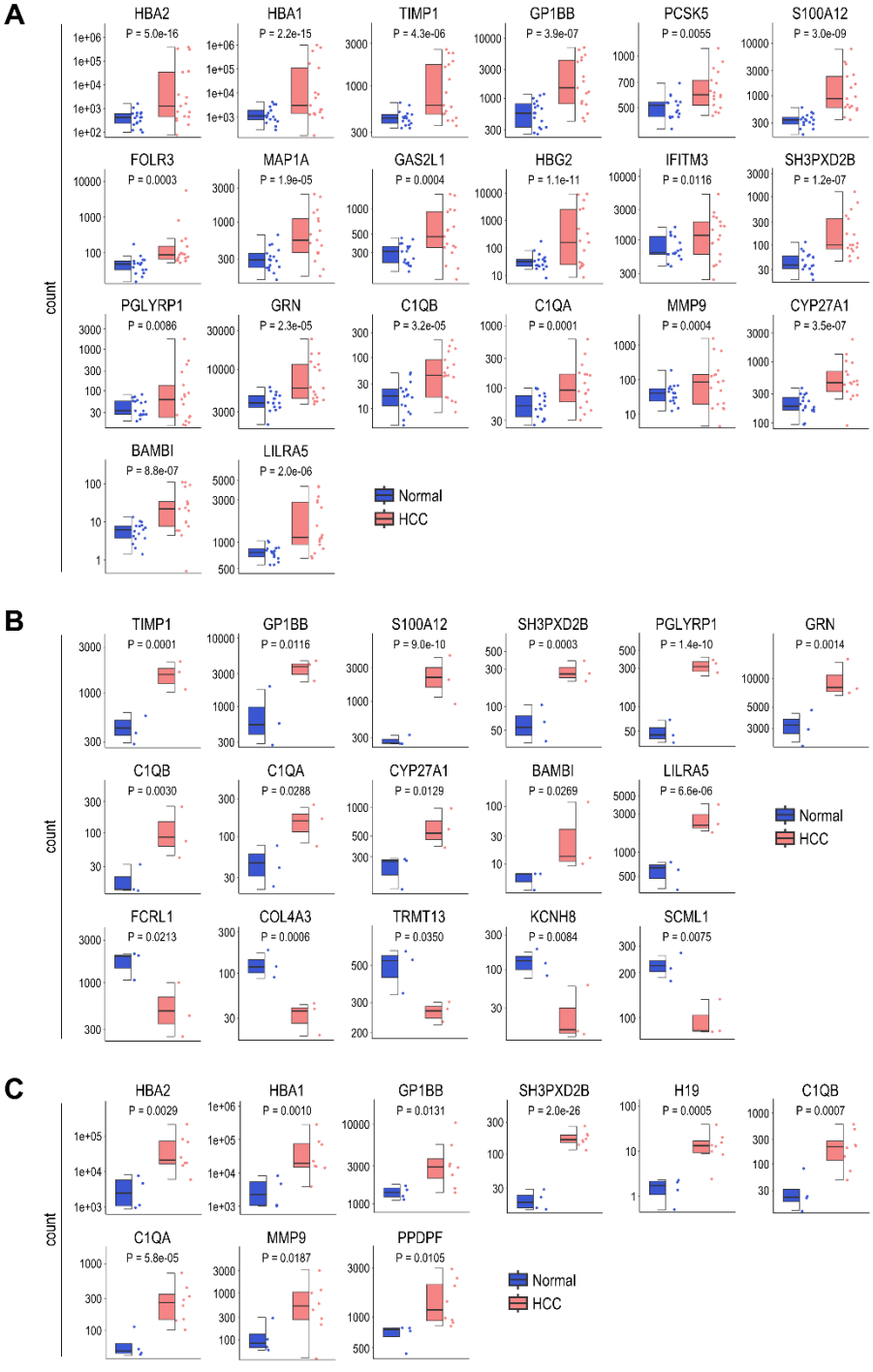
A
HBA2
P = 5.0e-16
HBA1
P = 2.2e-15
TIMP1
P = 4.3e-06
GP1BB
P = 3.9e-07
PCSK5
P = 0.0055
S100A12
P = 3.0e-09
FOLR3
P = 0.0003
MAP1A
P = 1.9e-05
GAS2L1
P = 0.0004
HBG2
P = 1.1e-11
IFITM3
P = 0.0116
SH3PXD2B
P = 1.2e-07
PGLYRP1
P = 0.0086
GRN
P = 2.3e-05
C1QB
P = 3.2e-05
C1QA
P = 0.0001
MMP9
P = 0.0004
CYP27A1
P = 3.5e-07
BAMBI
P = 8.8e-07
LILRA5
P = 2.0e-06
count
Normal
HCC
B
TIMP1
P = 0.0001
GP1BB
P = 0.0116
S100A12
P = 9.0e-10
SH3PXD2B
P = 0.0003
PGLYRP1
P = 1.4e-10
GRN
P = 0.0014
C1QB
P = 0.0030
C1QA
P = 0.0288
CYP27A1
P = 0.0129
BAMBI
P = 0.0269
LILRA5
P = 6.6e-06
FCRL1
P = 0.0213
COL4A3
P = 0.0006
TRMT13
P = 0.0350
KCNH8
P = 0.0084
SCML1
P = 0.0075
count
Normal
HCC
C
HBA2
P = 0.0029
HBA1
P = 0.0010
GP1BB
P = 0.0131
SH3PXD2B
P = 2.0e-26
H19
P = 0.0005
C1QB
P = 0.0007
C1QA
P = 5.8e-05
MMP9
P = 0.0187
PPDPF
P = 0.0105
count
Normal
HCC

Supplementary Figure S2. qPCR–AUC analysis of the identified DEGs for detection of early-stage HCC. (A, B) qRT–PCR and AUC results for the buffy coat DEGs. (A) C1QA results for HBV-HCC and NV-HCC patients. (B) SH3PXD2B results for HBV-HCC. (C-E) qRT–PCR and AUC results of DEGs from multiomics profiling. (C) LGALS1 results for HBV-HCC and NV-HCC patients. (D) LGALS9 results for HBV-HCC. (E) CD70 results for NV-HCC.

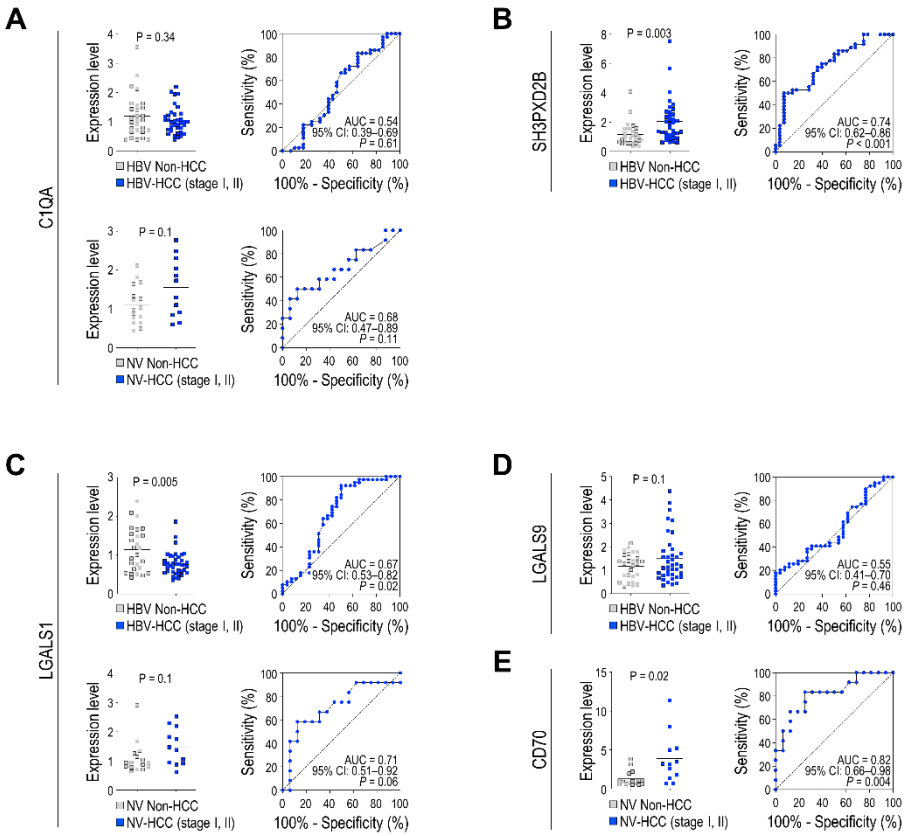
A
C1QA
Expression level
P = 0.34
HBV Non-HCC
HBV-HCC (stage I, II)
Sensitivity (%)
AUC = 0.54
95% CI: 0.39–0.69
P = 0.61
100% - Specificity (%)
P = 0.1
NV Non-HCC
NV-HCC (stage I, II)
AUC = 0.68
95% CI: 0.47–0.89
P = 0.11
B
SH3PXD2B
P = 0.003
AUC = 0.74
95% CI: 0.62–0.86
P < 0.001
C
LGALS1
P = 0.005
AUC = 0.67
95% CI: 0.53–0.82
P = 0.02
AUC = 0.71
95% CI: 0.51–0.92
P = 0.06
D
LGALS9
P = 0.1
AUC = 0.55
95% CI: 0.41–0.70
P = 0.46
E
CD70
P = 0.02
AUC = 0.82
95% CI: 0.66–0.98
P = 0.004

Supplementary Figure S3. Violin plots for DEG expression across different cell types. (A, B) Violin plots displaying the relative expression level of each significant DEG in each cell type. (A) DEGs from buffy coat WTS data. (B) DEGs from the buffy coat and plasma multiomics data.

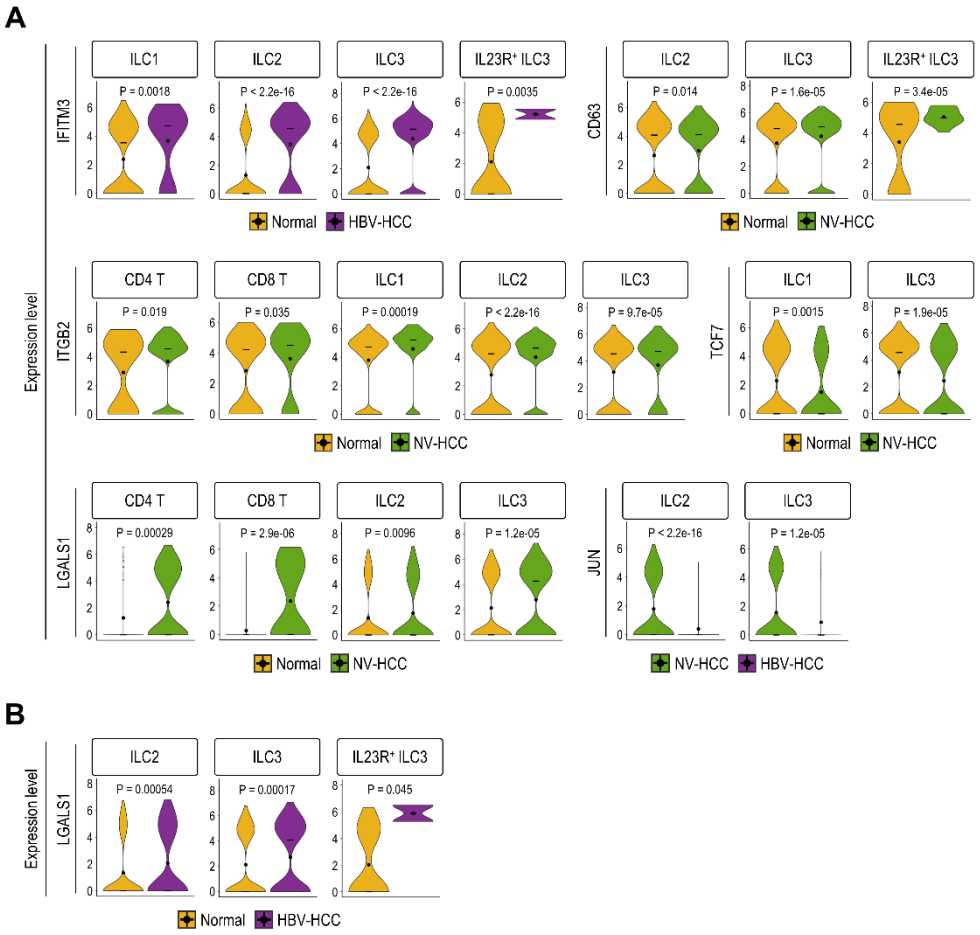
A
Expression level
IFITM3
ILC1
ILC2
ILC3
IL23R+ ILC3
P = 0.0018
P < 2.2e-16
P < 2.2e-16
P = 0.0035
Normal
HBV-HCC
CD63
ILC2
ILC3
IL23R+ ILC3
P = 0.014
P = 1.6e-05
P = 3.4e-05
Normal
NV-HCC
ITGB2
CD4 T
CD8 T
ILC1
ILC2
ILC3
P = 0.019
P = 0.035
P = 0.00019
P < 2.2e-16
P = 9.7e-05
Normal
NV-HCC
TCF7
ILC1
ILC3
P = 0.0015
P = 1.9e-05
Normal
NV-HCC
LGALS1
CD4 T
CD8 T
ILC2
ILC3
P = 0.00029
P = 2.9e-06
P = 0.0096
P = 1.2e-05
Normal
NV-HCC
JUN
ILC2
ILC3
P < 2.2e-16
P = 1.2e-05
NV-HCC
HBV-HCC
B
Expression level
LGALS1
ILC2
ILC3
IL23R+ ILC3
P = 0.00054
P = 0.00017
P = 0.045
Normal
HBV-HCC

Supplementary Figure S4. Single-cell analysis of CD70 and SH3PXD2B using extended datasets. (A) A Violin plot displaying relative expression of CD70 in the GSE179795 + GSE195648 dataset. (B) Box plots displaying relative expression of CD70 and SH3PXD2B in multiple datasets included in the ABC portal.

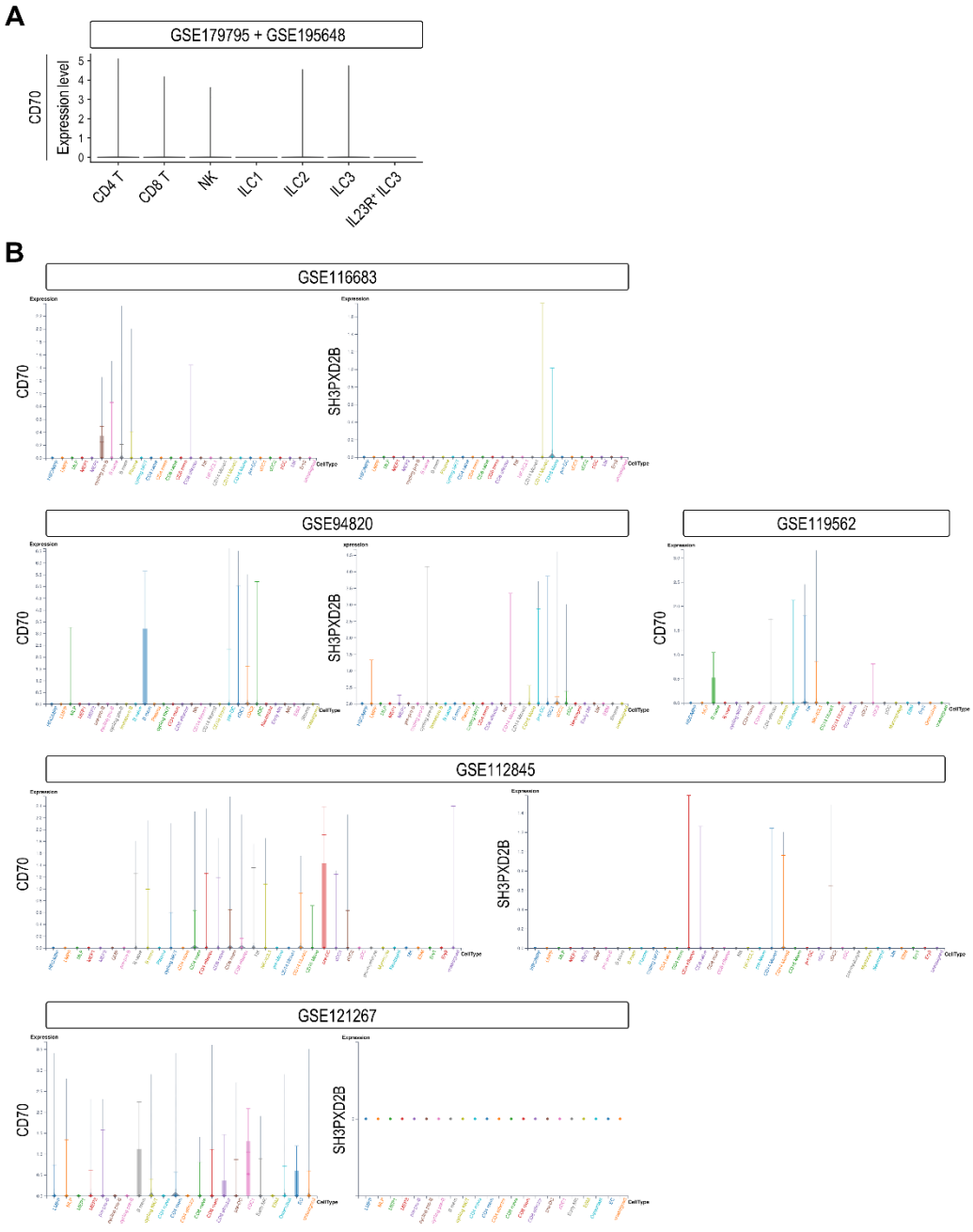
A
GSE179795 + GSE195648
CD70
Expression level
5
4
3
2
1
0
CD4 T
CD8 T
NK
ILC1
ILC2
ILC3
IL23R+ ILC3
B
GSE116683
CD70
SH3PXD2B
GSE94820
CD70
SH3PXD2B
GSE119562
CD70
GSE112845
CD70
SH3PXD2B
GSE121267
CD70
SH3PXD2B

Supplementary Table S1. Primer sequences for qRT–PCR.

Gene	Forward	Reverse
CD70	5’-TGTAACAGCTGGAACCTCAGT-3’	5’-TGGATGCAAGATGCGGGATT-3’
LGALS1	5’-AGCAGCGGGAGGCTGTCTTTC-3’	5’-ATCCATCTGGCAGCTTGACGGT-3’
LGALS9	5’-AGTCCAGCTGTCCCCTTTTC-3’	5’-CACACCACGTACCCTCCATC-3’
SH3PXD2B	5’-TCAGGTTGGTGGTTCGTCAG-3’	5’-TCTCCTCTTCTTCAGGCTGC-3’
C1QA	5’-GAGTTGACAACAGGAGGCAGAG-3’	5’-CTTTCTTCCCGTCTGGTGCT-3’
GAPDH	5’-AGTATGACAACAGCCTCAAG-3’	5’-TCATGAGTCCTTCCACGATA-3’

Supplementary Table S2. Baseline characteristics of the included patients.

Variables	Buffy coat WTS data (N=175)		Targeted proteome data (N=58)	
	HCC (N=129)	Non-HCC (N=46)	HCC (N=52)	Normal (N=6)
Male, n (%)	107 (82.9)	34 (73.9)	41 (78.8)	1 (16.7)
Age, mean ± SD	59.1 ± 12.0	49.3 ± 13.6	60 ± 10.5	30.0 ± 3.9
Etiology				
Viral (HBV) , n (%)	95 (73.6)	29 (63)	43 (82.7)	
Non-viral, n (%)	34 (26.4)	17 (37)	9 (17.3)	
Cirrhosis, n (%)	109 (84.5)	15 (32.6)	46 (88)	
Platelet, mean ± SD	174.8 ± 77.1	202.6 ± 75.7	176.7 ± 78.7	220.7 ± 61.0
AST, mean ± SD	62.4 ± 65.0	53.7 ± 35.0	53.4 ± 32.5	17.5 ± 0.7
ALT, mean ± SD	42.6 ± 44.9	65.0 ± 61.5	39.0 ± 28.5	12.5 ± 0.7
Albumin, mean ± SD	4.2 ± 0.6	4.6 ± 0.5	4.2 ± 0.4	4.4 ± 0.9
Bilirubin, mean ± SD	1.3 ± 2.8	0.7 ± 0.4	0.8 ± 0.6	0.5 ± 0.4
AFP, mean ± SD	2898.7 ± 7630.1	8.2 ± 15.6	3048.3 ± 8802	1.4 ± 0.5
PT, mean ± SD	13.5 ± 2.2	13.2 ± 1.5	13.1 ± 1.3	

WTS, whole transcriptome sequencing; HCC, hepatocellular carcinoma; SD, standard deviation; HBV, hepatitis B virus; AST, aspartate aminotransferase; ALT, alanine aminotransferase; AFT, alpha-fetoprotein; PT, prothrombin time.

Supplementary Table S3. Clinical information of the patients in the validation datasets.

Variables	VD1 (PRJNA739257)		VD2 (PRJNA909469)		VD3 (PRJNA717231)	
	Normal	HCC	Normal	HCC	Normal	HCC
Sample, n	17	17	3	3	4	8
Sex						
Male, n		11	3	3	2	6
Female, n		6	0	0	2	2
Age, mean ± SD		53 ± 19	47 ± 6	62 ± 21	29 ± 4	64 ± 4
Etiology		HBV		HBV		HBV
BCLC						
Stage A, n		6		0		4
Stage B, n		1		0		4
Stage C, n		4		0		0
Stage D, n		5		3		0
Cirrhosis, n		9				
Metastasis, n		9				
Race			Asian	Asian		
Patient source	Shenzhen Traditional Chinese Medicine Hospital		Shenzhen Traditional Chinese Medicine Hospital		King Chulalongkorn Memorial Hospital, Thailand	
Sample type	PBMC		PBMC		PBMC	
Sample isolation	1. PB 2ml collection (EDTA blood) 2. PBMCs separation (Ficoll-Paque PREMIUM) 3. RNA extraction (TRIzol)		1. PB 8ml collection (EDTA anti-coagulant vacuum angiography) 2. PBMCs isolation (density gradient centrifugation) 3. RNA extraction (TRIzol)		1. PB 6ml collection (EDTA blood) 2. PBMCs isolation (Percoll PLUS density gradient media) 3. RNA extraction (TRIzol)	
Data type	Bulk RNA-seq		Bulk RNA-seq		Bulk RNA-seq	

VD, validation dataset; HCC, hepatocellular carcinoma; SD, standard deviation; HBV, hepatitis B virus; PBMC, peripheral blood mononuclear cell; PB, peripheral blood.